Geoderma 469 (2026) 117816

Contents lists available at ScienceDirect

Geoderma

journal homepage: www.elsevier.com/locate/geoderma

From buffering to collapse: a hump-shaped rhizosphere response to shelterbelt forest degradation

Guan Wang [a,*], Huijie Xiao [a], Linlin Shi [a], Tianshuo Liu [a], Chenxi Yang [a,e], Zhiming Xin [a,b,c], Junran Li [d]

[a] School of Soil and Water Conservation, Beijing Forestry University, Beijing 100083, China
[b] Experimental Center of Desert Forestry, Chinese Academy of Forestry, Dengkou 015200, China
[c] Inner Mongolia Dengkou Desert Ecosystem National Observation Research Station, National Forestry and Grassland Administration, Dengkou 015200, China
[d] Department of Geography, The University of Hong Kong, 999077, Hong Kong Special Administrative Region of China
[e] School of Earth System Science, Tianjin University, Tianjin 300072, China

ARTICLE INFO

Handling Editor: Tessa Camenzind

Keywords:
Rhizosphere effect
Shelterbelt degradation
Nonlinear response
Buffering-collapse threshold
Plant-soil feedbacks

ABSTRACT

Forest degradation is widely assumed to drive a monotonic decline in belowground functioning, yet plant-soil feedbacks may transiently buffer stress. We tested this idea by quantifying the rhizosphere effect (RE), the percentage difference between rhizosphere and bulk soil, for soil carbon (C), nitrogen (N) and phosphorus (P) pools, enzymatic activities, and microbial biomass across four degradation stages in three types of shelterbelt forests. We found that REs generally increased or remained stable from undegraded to mild-moderate degradation stage and then declined sharply at severe degradation stage. This nonlinear pattern was consistent across species but differed in amplitude and timing, with *Populus thevestina* showing the largest early increases, *Populus alba* maintaining RE longer before decline, and *Populus popularis* reaching negative REs for SOC and microbial biomass phosphorus at the severe degradation stage. Early positive RE coincided with lower pH and higher water-soluble organic carbon (WSOC), soil water content (SWC), and enriched available N (NH_4^+ and NO_3^-) in rhizospheres, conditions that stimulate microbial activities and nutrient turnover. As degradation intensified, the significant differences between rhizosphere and bulk soil properties contracted and eventually disappeared, reflecting a decline of plant-soil feedbacks likely driven by reduced root exudation. Random-forest and redundancy analyses highlighted rhizosphere P, rhizosphere N, bulk soil WSOC, rhizosphere SWC, and bulk-soil stoichiometry as the most influential factors of these shifts, consistent with a transition from compensatory stimulation to functional collapse beyond a critical tipping zone. This study provides the first field evidence that rhizosphere functioning responds nonlinearly to forest degradation. Recognizing this transient compensatory phase advances our understanding of ecosystem belowground resilience and can inform the intervention windows for dryland forest restoration.

1. Introduction

The rhizosphere, the narrow zone (~2 mm) of soil surrounding the plant roots, is one of the most dynamic regions in forest ecosystems (Dotaniya and Meena, 2015; Lv et al., 2023). Driven by root-microbe-soil interaction, rhizosphere receives substantial root exudates (e.g. carbohydrates, organic acids, amino acids, and mucilage) and harbors a dense and diverse community of microorganisms, facilitating soil nutrient cycling and altering soil properties (Pett-Ridge and Firestone, 2017; Ling et al., 2022; Bouwmeester et al., 2025). As a result, the rhizosphere is typically characterized by enhanced nutrient availability, elevated enzymatic activity, and higher microbial biomass than bulk soil (Dotaniya and Meena, 2015; Friggens et al., 2025). This phenomenon, known as the rhizosphere effect (RE), was proposed to describe the differential biological and physicochemical properties of rhizosphere soil compared to the surrounding bulk soil (Jones et al., 2009; Dotaniya and Meena, 2015). Understanding of the RE provides key insights into the capacity of plant roots to actively forage for nutrients, modify their

* Corresponding author at: Beijing Forestry University, No. 35 East Qinghua Street, Beijing 100083, China.
E-mail addresses: Wanggbjfu@bjfu.edu.cn (G. Wang), herr_xiao@hotmail.com (H. Xiao), 19712971376@163.com (L. Shi), bjfu_lts1231@163.com (T. Liu), yangchenxi922@163.com (C. Yang), xzmlkn@163.com (Z. Xin), lijr@hku.hk (J. Li).

https://doi.org/10.1016/j.geoderma.2026.117816
Received 4 November 2025; Received in revised form 9 April 2026; Accepted 11 April 2026

immediate soil environment, and regulate belowground ecological processes (Lambers et al., 2009; Hill and Jones, 2019).

In forest ecosystems, the rhizosphere serves as a critical interface for nutrient acquisition, carbon (C) mobilization, and water absorption, all of which are fundamental to tree health and forest productivity (Pii et al., 2015; Baldrian, 2017; Williams and de Vries, 2020). Furthermore, the rhizosphere's high responsiveness to environmental fluctuations makes it a sensitive indicator of plant physiological status and ecosystem resilience (Mori et al., 2013; Preece and Peñuelas, 2016). As forests undergo environmental stresses such as nutrient limitation, drought, elevated CO_2, or anthropogenic disturbance, the intensity of plant-soil interactions in the rhizosphere can shift markedly (Sardans and Peñuelas, 2013; Zhao et al., 2022). For instance, Meier et al. (2015) reported increased N-releasing enzyme activity in the rhizosphere under elevated CO_2, reflecting adaptive root strategies to enhance nutrient availability under changing atmospheric conditions. Investigating REs along gradients of forest change is therefore essential for understanding the trajectory of belowground ecosystem function, assessing the forest's reaction capacity when facing stresses, and informing management strategies for ecological restoration and sustainable development (Meier et al., 2019).

Shelterbelt forests represent a special type of forest ecosystem, widely distributed across arid and semi-arid regions worldwide (Zhu and Song, 2021; Cheng et al., 2021). These human-established forest networks are designed to regulate microclimates, reduce soil erosion, combat desertification, and protect agricultural lands and residential areas from wind disasters (Liang et al., 2022; Xie et al., 2024). However, due to climate change, water deficiency, and inappropriate management practices, over 50% of shelterbelt forests are facing degradation characterized by canopy dieback, withered branch, slow growth rate, and high mortality (Chirwa and Mahamane, 2017; Cao et al., 2021; Wang et al., 2024). Previous studies have documented the structural and physiological changes in aboveground components of shelterbelt degradation, especially in the northern China (Liu et al., 2020; Liang et al., 2024; Wen et al., 2024). However, the belowground responses, particularly the functional dynamics of the rhizosphere during degradation process, remain poorly understood (Freschet et al., 2021; George et al., 2024). Most existing studies arbitrarily assumed a monotonic decline of plant-soil interaction during forest degradation, overlooking the possibility of buffering effects, such as elevated root exudation and stimulated microbial mineralization caused by plant compensatory responses, before a total collapse (Robert et al., 2014; Cross and Harte, 2007). Without incorporating these mechanisms and temporal complexity in root-soil feedbacks, predictions of degraded shelterbelt ecosystem trajectories remain deficient and may misguide restoration strategies (Prescott, 2022; Zhang et al., 2023).

The functional dynamics of the rhizosphere during forest degradation are likely governed by shifts in plant C allocation and metabolic priorities (Prescott, 2022; Zhang et al., 2026). Under initial environmental stress, such as the water deficiency or nutrient limitation that triggers early-stage shelterbelt degradation, plants might employ a buffering strategy. This involves reallocating nonstructural carbohydrates to enhance root exudation and stimulate microbial mineralization, thereby maintaining relatively steady nutrients and water acquisition despite deteriorating conditions (Shen et al., 2020; Williams and de Vries, 2020; Brunn et al., 2022, 2025). However, as degradation progresses toward severe stages, persistent canopy dieback and reduced photosynthetic capacity may eventually trigger C starvation (Anderegg et al., 2012; Wiley, 2020). This exhaustion of internal carbohydrates may subsequently limit the energy available for rhizodeposition, reducing microbial activity and nutrient turnover in the rhizosphere (Millard et al., 2007; Clausing et al., 2021). This transition from stress-induced stimulation to resource-limited collapse may result in a nonlinear response of the RE along the degradation gradient. Accordingly, we hypothesized that the RE would follow a nonlinear trajectory: initially increasing or remaining stable due to stimulated root and microbial activity, but declining under severe degradation as plant-soil feedbacks weaken and rhizosphere functionality collapses.

To test this hypothesis, we conducted a field-based study in shelterbelt forests of northern China, spanning four levels of degradation and three widely planted poplar species. Our goal was to determine how RE changes along the degradation gradient, and to identify the primary soil and plant drivers of these shifts. By explicitly contrasting rhizosphere and bulk soils across the degradation stages, this study advances understanding of belowground functioning in forest ecosystems and establishes a new framework for interpreting rhizosphere processes as early indicators of forest resilience loss, informing the sustainable management and restoration of widely distributed shelterbelt ecosystems.

2. Methods

2.1. Site description

This study was conducted in the Desert Forestry Experimental Center of the Chinese Academy of Forestry, situated in Dengkou County, Inner Mongolia Autonomous Region, northern China (40°17′–40°29′N, 106°35′–106°59′E). The site lies on the northeastern edge of the Ulan Buh Desert and is characterized by a mosaic of desert oases (Fig. S1), with the Yellow River flowing through the county's eastern boundary. The region has a temperate continental climate (Yan et al., 2025). Annual precipitation is low, averaging 134 mm and mainly occurred between June and September. The mean annual temperature is 7.6 °C, and the area receives abundant sunlight, with approximately 3000 h of sunshine per year (Yu et al., 2018). Prevailing winds are mainly from the northwest and southwest, averaging 3 m/s (Wang et al., 2024). Soils at the study site are classified as Arenosols (IUSS Working Group WRB, 2022), characterized by sandy texture (>60% sand), weak profile development, low nutrient retention, and poor water-holding capacity (Cao et al., 2021).

Artificial grid-shaped shelterbelts have been established for over 30 years around desert oases, using drought-tolerant tree species to mitigate wind erosion and stabilize the soils (Fig. S1). Poplars (*Populus* spp.) are a key component of these plantations due to their rapid growth, drought tolerance, and ability to develop dense root systems that enhance soil stabilization (Brandle et al., 2021). The three most widely planted species, *Populus popularis, Populus thevestine, and Populus alba*, have formed three distinct, single-species shelterbelt types (Fig. S1). All shelterbelts follow a uniform structural design, with three parallel tree rows (total width of 8 m), consisting of 4-meter spacing between rows and 4 m between individual trees within a row. Fertilizers were applied only during the initial seedling establishment phase, with no subsequent inputs over the past 30 years. These shelterbelt networks enclose the inner oases, which are composed of croplands and residential areas. The dominant crops are *Zea mays L.* (maize), *Cucurbita pepo L.* (squash), and *Helianthus annuus L.* (sunflower). A buffer zone of approximately 5 m separates the shelterbelt tree lines from the adjacent croplands.

2.2. Experimental methods

From July 21 to August 25, 2024, we conducted a field survey in the study area to evaluate the status of shelterbelt networks, focusing on three types of widely distributed pure Populus shelterbelts, including *Populus popularis*, *Populus thevestina*, and *Populus alba*. Shelterbelt degradation stages were classified based on the proportion of dead branches, following Marais et al. (2022) and Liang et al. (2024). Four degradation stages were defined: undegraded (Level 1, <10% dead branches), mildly degraded (Level 2, 10–25%), moderately degraded (Level 3, 25–50%), and severely degraded (Level 4, >50%). Tree height, diameter at breast height (DBH), and crown width were used as supplementary indicators to confirm consistency with the visually estimated degradation levels (Table 1). To ensure adequate replication and

Table 1
Degradation stage classification of the three types of shelterbelt forests.

Tree species	Degradation stage	Classification of dead branch rate (%)	Dead branch rate (%)	Tree height (m)	DBH (cm)	Crown width (m)
Populus popularis	1	<10	3.80 ± 1.30	11.9 ± 0.26	39.3 ± 3.04	7.07 ± 0.82
	2	10–25	12.2 ± 1.79	9.50 ± 0.35	42.4 ± 2.46	4.55 ± 0.40
	3	25–50	30.2 ± 3.53	8.60 ± 0.42	31.9 ± 1.58	2.95 ± 0.63
	4	>50	62.5 ± 7.58	7.20 ± 0.57	27.2 ± 2.97	2.58 ± 0.42
Populus thevestina	1	<10	5.20 ± 1.79	13.3 ± 0.41	41.1 ± 4.52	5.41 ± 0.84
	2	10–25	12.8 ± 2.17	11.9 ± 0.22	37.2 ± 3.99	4.17 ± 0.49
	3	25–50	33.0 ± 3.53	10.7 ± 0.22	33.9 ± 1.35	3.17 ± 0.88
	4	>50	60.0 ± 7.90	9.53 ± 0.42	31.5 ± 5.14	2.66 ± 0.35
Populus alba	1	<10	3.60 ± 1.34	12.2 ± 0.48	39.7 ± 4.53	4.26 ± 0.53
	2	10–25	13.0 ± 3.46	9.82 ± 0.43	38.1 ± 8.12	3.33 ± 0.57
	3	25–50	43.5 ± 5.70	9.56 ± 0.46	36.3 ± 5.00	2.63 ± 0.83
	4	> 50	75.0 ± 7.90	8.45 ± 0.14	34.9 ± 5.30	2.48 ± 0.41

Note: all the data are expressed as mean ± standard deviation.

account for spatial heterogeneity, nine spatially independent sampling units were established across the study area, with three units for each tree species. Within each sampling unit, four plots (5 m × 20 m each) representing different degradation stages were selected. In subsequent statistical analyses, these sampling units were treated as blocks and included as a random effect nested within tree species to account for spatial non-independence. In total, 36 plots were sampled. A detailed overview of the study area, spatial layout, and representative photographs is provided in Fig. S1.

Within each plot, bulk soil samples were carefully collected using five-points sampling method from the surface layer (0–10 cm) and thoroughly mixed to form one composite sample. The composite sample was then sieved through a 2 mm mesh to remove roots, debris, and gravel. Within each standardized plot, we selected five well-growing trees exhibiting comparable DBH and tree height, aligning with the mean DBH and tree height characteristic of their respective shelterbelt type. We carefully excavated the fine roots (<2 mm) from the topsoil layer near the tree base (20–50 cm from the trunk) on the four cardinal directions (north, south, east, and west). Rhizosphere soils were gently brushed over a sterile container (Barillot et al., 2013). Then, the collected rhizosphere soil was sieved through a 2 mm mesh to remove coarse debris and homogenized to be one composite rhizosphere soil sample of the certain plot (Barillot et al., 2013; Herre et al., 2022). Thus, we collected 36 bulk soil samples and 36 rhizosphere soil samples in total. Each soil sample was subsequently divided into two subsamples: one was stored at 4 °C for analysis of microbial activity and enzyme assays, the other was air-dried for the assessment of physicochemical properties.

2.3. Laboratory analysis

Soil pH was determined at a 1:2.5 soil: water ratio using a DMP-2 mV/pH detector. Soil water content (SWC) was measured using the gravimetric oven-drying method (Wang et al., 2024). Soil organic carbon (SOC) was analyzed using the combustion method by a TOC analyzer (model N/C 3100, Analytik Jena, Germany). Water soluble organic carbon (WSOC) was extracted with ultrapure water using a soil: water ratio of 1:5. The supernatant was filtered through 0.45-μm membrane filters, and analyzed through combustion method by a TOC analyzer (model N/C 3100, Analytik Jena, Germany). For soil total nitrogen (TN), samples were digested with sulfuric acid and a mixed catalyst, and the N content was determined using a Kjeldahl nitrogen analyzer (KDY-9380, KETUO) (Wu et al., 2022). Soil total phosphorus (TP) was measured through the digestion of samples with $HCLO_4$-H_2SO_4, followed by colorimetric analysis using the molybdenum blue method (Wu et al., 2022). Soil ammonium (NH_4^+) and nitrate (NO_3^-) concentrations were determined using 2 M KCl extraction followed by colorimetric analysis with a continuous flow analyzer (SAN++ Compact V2, Skalar, Netherlands).

To assess the soil enzyme activities associated with soil C, N, and P cycling, we measured the activities of β-glucosidase (BG), N-acetyl-β-D-glucosaminidase (NAG), and neutral phosphatase (Ppase) in soil samples using a fluorometric assay with 4-methylumbelliferone (MUF)-linked substrates, following protocols of Hendel and Marxsen (2020) and German et al. (2011), with modifications for neutral pH conditions. Fresh soil (1 g) was suspended in 125 mL of 50 mM Tris buffer (pH 7.0) and homogenized. For each enzyme, 200 μL of the soil slurry was dispensed into black 96-well microplates along with 50 μL of the appropriate MUF-substrate. Microplates were incubated at 25 °C in the dark for 2 h, after which fluorescence was measured using a microplate reader at excitation 365 nm and emission 450 nm. Enzyme activity was calculated as μmol g^{-1} soil h^{-1} for BG and NAG, and μmol g^{-1} soil 24 h^{-1} for Ppase (German et al., 2011).

Soil microbial biomass carbon (SMBC) and nitrogen (SMBN) were extracted using 0.5 mol L^{-1} K_2SO_4 following chloroform fumigation. SMBC was measured using a total organic carbon analyzer (model N/C 3100, Analytik Jena, Germany) (Ashraf et al., 2020). For SMBN, the extracts were oxidized with potassium persulfate, and N concentration was determined by UV spectrophotometry at 220 nm and 275 nm (Stevenson et al., 2016). Microbial biomass phosphorus (SMBP) was extracted with 0.5 mol L^{-1} $NaHCO_3$ after chloroform fumigation and quantified using the molybdenum blue colorimetric method at 700 nm (Chen et al., 2025).

2.4. Statistical analysis

The RE of each soil property was calculated using the following equation (Kuzyakov and Razavi, 2019).

$$Rhizosphere\ Effect\ (RE) = \frac{X_r - X_b}{X_b} \times 100\%$$

where X_r is the value of the soil property in rhizosphere soil, X_b is the corresponding value in bulk soil. The unit of the RE is %. RE > 0 indicates a positive RE, representing the enrichment or stimulation of the property in the rhizosphere. RE = 0 indicates no effect. RE < 0 indicates a negative RE, reflecting depletion or suppression of the property in the rhizosphere.

Statistical analyses were performed using R 4.3.3 (R Core Team, 2024). All variables were checked for normality and homogeneity of variance before analysis. To account for the spatial structure of the sampling design, linear mixed-effects models were fitted using the lme4 package (Bates et al., 2015). Because blocks were not shared among tree species, block was treated as a random effect nested within tree species. For RE variables shown in Fig. 1, tree species, degradation stage, and

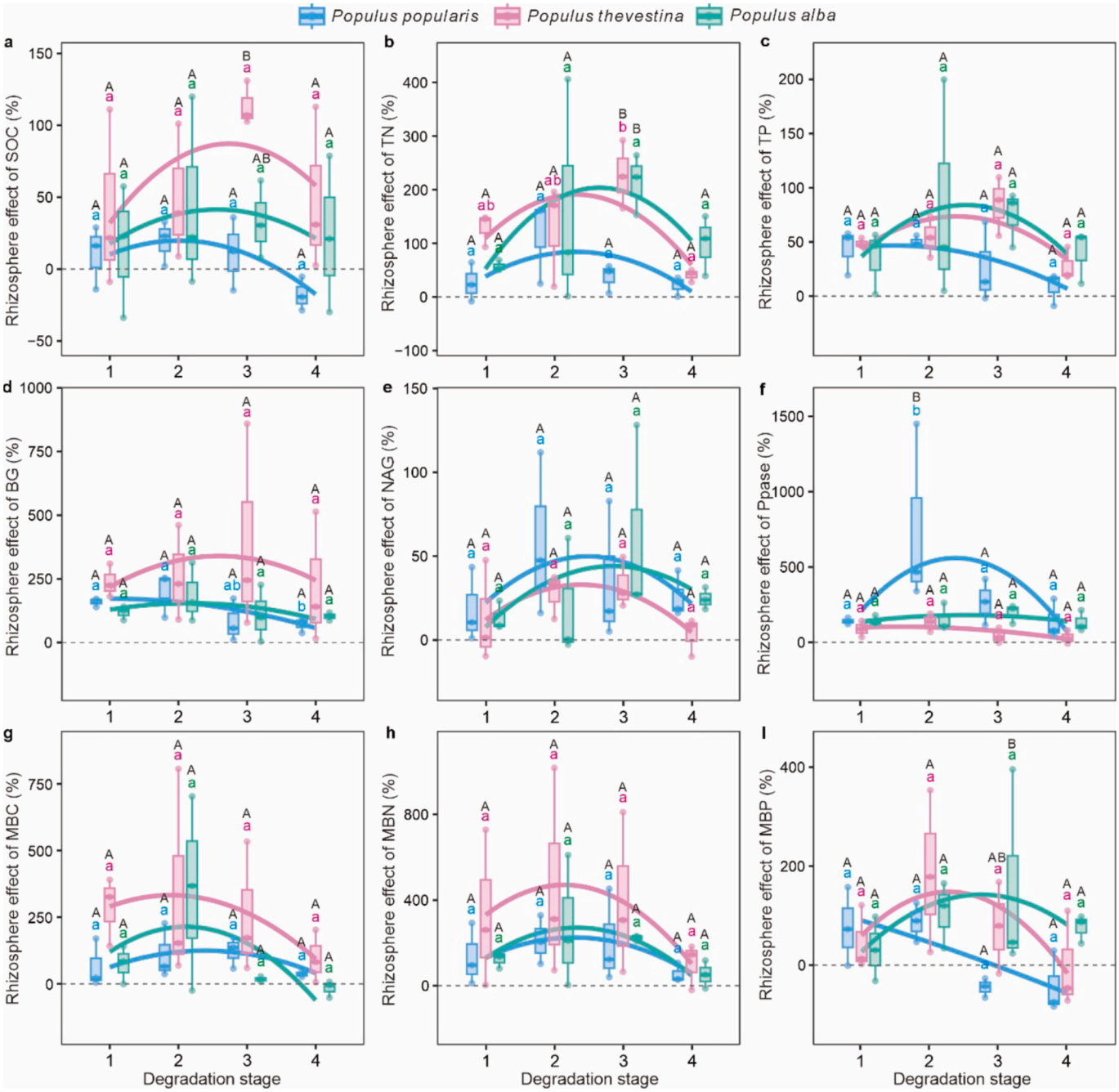

Fig. 1. The rhizosphere effect values of soil C, N, and P contents, soil enzymatic activities, and soil microbial biomass in the four different degradation stages of the three types of shelterbelt forests. Degradation stages 1, 2, 3, 4 refer to undegraded, mildly degraded, moderately degraded, and severely degraded shelterbelts, respectively. The colored lowercase letters indicate significant differences among degradation stages within each tree species, whereas uppercase letters indicate significant differences among the three tree species within each degradation stage ($p < 0.05$), based on linear mixed-effects models followed by estimated marginal means with Tukey adjustment. The colored curves show the fitted quadratic polynomial curves for the three types of shelterbelt forests, with blue, pink, and green colors representing *Populus popularis, Populus thevestina,* and *Populus alba* pure shelterbelts, respectively.

their interaction were included as fixed effects, and block nested within tree species was included as a random effect. For soil variables shown in Fig. 2, tree species, degradation stage, soil type, and their interactions were included as fixed effects, with the same nested random structure. The significance of fixed effects was evaluated using the lmerTest package (Kuznetsova et al., 2017). Post hoc comparisons were conducted using estimated marginal means with Tukey adjustment using emmeans package (Lenth and Piaskowski, 2026), with $p < 0.05$ considered statistically significant. To visualize trends during degradation process, quadratic polynomial curves ($y \sim poly(x, 2)$) were fitted separately for each tree species across degradation stages. The detailed results of the linear mixed-effects models are presented in Table S1 and Table S2, corresponding to Fig. 1 and Fig. 2, respectively.

A random forest model was used to quantify the explained variations of each RE with the rest of variables, using the randomForest package in R (Liaw and Wiener, 2002). Significance of the model was assessed with 5000 permutations of the response variable using the A3 package (Scott, 2012). The levels of significant influential predictors for each RE were marked based on increase in mean squared error (%IncMSE), with double asterisk (**) indicating highly important variables (%IncMSE >

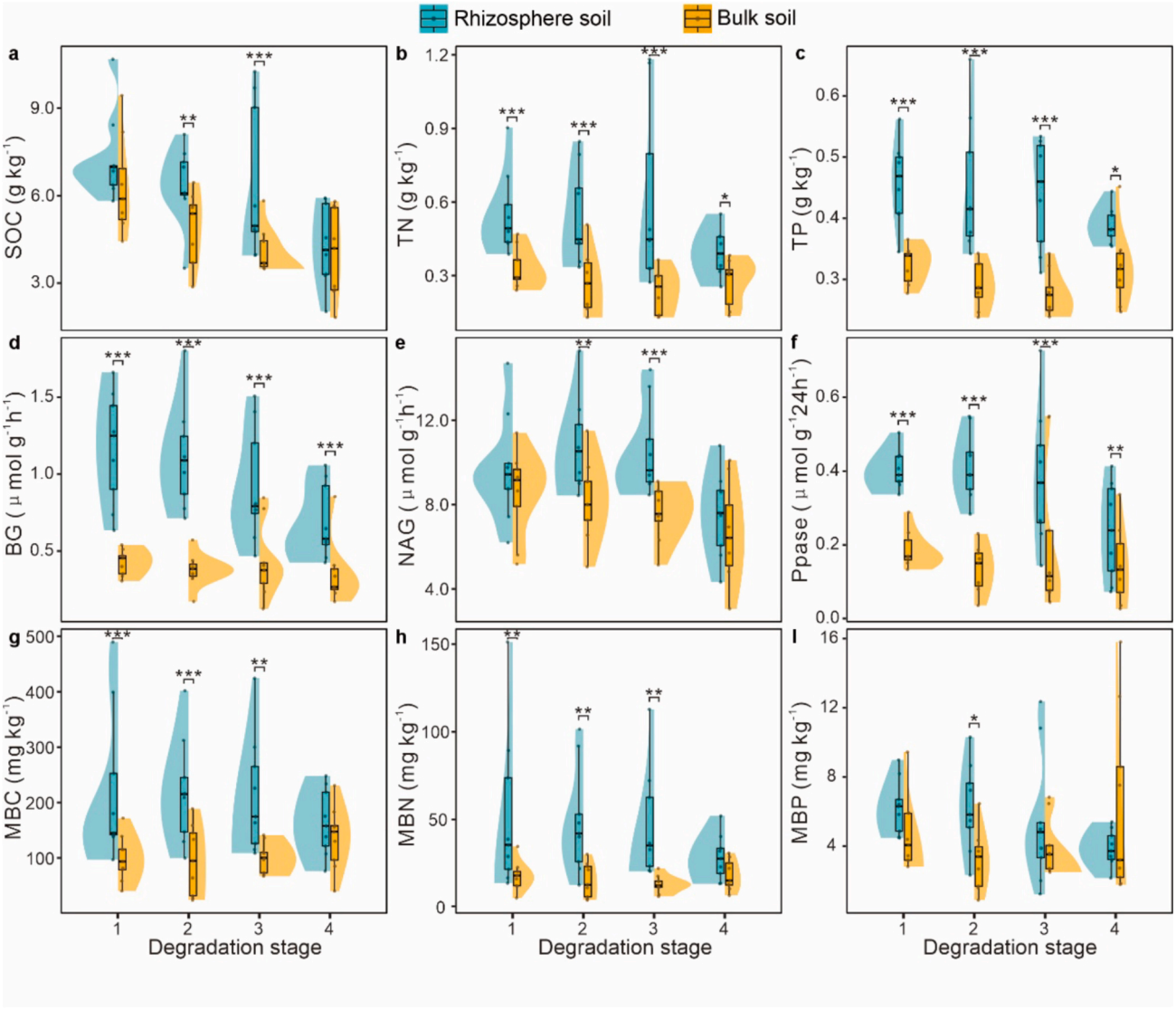

Fig. 2. The soil C, N, and P contents, soil enzymatic activities, and soil microbial biomass of the rhizosphere soil and bulk soil in the four different degradation stages of the shelterbelt forests. Degradation stages 1, 2, 3, 4 refer to undegraded, mildly degraded, moderately degraded, and severely degraded shelterbelts, respectively. Data are combined across the three *Populus* species, with $n = 9$ for each degradation stage and soil type. Asterisks indicate significant differences between rhizosphere and bulk soil within each degradation stage (*** $p < 0.001$, ** $p < 0.01$, * $p < 0.05$), based on linear mixed-effects models with block nested within tree species, followed by estimated marginal means with Tukey adjustment.

10), single asterisk (*) indicating moderately important variable ($5 <$ % IncMSE ≤ 10), and no asterisk representing less important variable (% IncMSE ≤ 5). All the figures were performed using the ggplot2 package (Wickham, 2016).

Additionally, redundancy analysis (RDA) was conducted to evaluate how key environmental variables influenced the multivariate patterns of the RE variables. The explanatory variables included selected soil physicochemical and enzymatic properties from both rhizosphere and bulk soils, which were identified as important predictors based on a preceding random forest analysis. Prior to RDA, explanatory variables were standardized (z-score transformation) to ensure comparability among variables. The RDA was first performed on the combined dataset including all three poplar species to examine overall patterns, and subsequently conducted separately for each species to better resolve species-specific responses along the degradation gradient. All analyses were performed in R using the vegan package (Oksanen et al., 2024).

3. Results

3.1. Rhizosphere effect across shelterbelt degradation

The REs of nine soil properties, including three for soil nutrient elements, three for soil enzymatic activities, and three for microbial biomass, varied across shelterbelt degradation stages. For soil SOC, RE patterns differed notably by species (Fig. 1a). In *Populus popularis*, the RE of SOC remained relatively stable through the early stages before exhibiting a downward trend under severe degradation. *Populus thevestina* followed a more pronounced nonlinear trajectory, with the RE increasing from the undegraded to the moderately degraded stage, followed by a sharp decline during severe degradation. In contrast, *Populus alba* exhibited only minor fluctuations throughout the degradation gradient. Species differences were most pronounced at the moderately degraded stage, where *Populus thevestina* had significantly higher RE of SOC than *Populus popularis* (Fig. 1a).

The RE of TN followed a broadly similar trend across all poplar species, with values rising from early to mid-degradation before

declining sharply under severe degradation (Fig. 1b). However, the timing of peak RE varied. *Populus popularis* exhibited its highest RE value at the mildly degraded stage, whereas *Populus thevestina* and *Populus alba* reached their peak RE values at the moderately degraded stage (Fig. 1b). For TP, the variations between stages were less pronounced for all three types of shelterbelts (Fig. 1c).

Enzyme activities also showed species-specific responses (Fig. 1d–f). The RE of BG in *Populus popularis* maintained unchanged at early degradation stage and decreased significantly thereafter, while *Populus thevestina* and *Populus alba* showed slight early increases before returning to initial levels (Fig. 1d). The RE of NAG generally followed a nonlinear pattern across all shelterbelt types, increasing during early degradation before undergoing a sharp decline (Fig. 1e). *Populus popularis* reached its highest value at the mildly degraded stage, whereas *Populus thevestina* and *Populus alba* peaked at the moderately degraded stage (Fig. 1e). For Ppase, *Populus popularis* displayed a significant early increase in RE from the undegraded to mildly degraded stage before declining, whereas *Populus thevestina* and *Populus alba* exhibited minimal variation throughout the degradation process (Fig. 1f).

Regarding soil microbial biomass, the REs of MBC and MBN in *Populus popularis and Populus alba* shelterbelts increased from the healthy to moderately degraded stages before declining at the severe degradation stage, while *Populus thevestina* remained relatively stable during the early stages of degradation before dropping sharply in severe degradation (Fig. 1g, h). Across all degradation levels, *Populus thevestina* consistently exhibited the highest REs of MBC and MBN among the three species. For MBP, the RE in *Populus popularis* shifted from positive to negative values after mildly degraded stage (Fig. 1i). In contrast, *Populus thevestina* showed an early increase in RE of MBP followed by a gradual decline, though the value remained positive throughout the gradient. In *Populus alba* shelterbelts, while the RE of MBP fluctuated across degradation stages without clear stage differences, this species maintained the highest RE of MBP under moderate degradation compared to the other two shelterbelt types.

3.2. The dynamics of rhizosphere and bulk soils during shelterbelt degradation

Rhizosphere soil pH was consistently and significantly lower than bulk soil across all species and degradation stages (Table 2). While SWC was generally higher in the rhizosphere than in the bulk soil, it decreased significantly with increasing degradation stage in the rhizosphere of *Populus popularis* and *Populus thevestina* shelterbelts (Table 2). Concentrations of available N (NH_4^+ and NO_3^-) are also displayed here, as they represent the most limiting nutrients in shelterbelt ecosystems of this arid region (Wang et al., 2024). The NH_4^+ showed little variations in *Populus popularis* and *Populus alba* shelterbelts. In contrast, *Populus thevestina* exhibited a significant increase in rhizosphere NH_4^+ at the moderately degraded stage, where it was also significantly high than its corresponding bulk soil. Similarly, NO_3^- levels were consistently and significantly higher in the rhizosphere than in the bulk soil of *Populus thevestina* shelterbelts across all degradation stages. In *Populus alba* shelterbelts, rhizosphere NO_3^- decreased significantly as degradation progressed, whereas no significant change was detected in the bulk soil (Table 2).

Soil total nutrients were generally higher in the rhizosphere than in bulk soil (Fig. 2). SOC declined progressively in both rhizosphere and bulk soils along the degradation gradient. Although SOC levels were generally comparable between the two soil compartments during early stages, rhizosphere SOC became significantly higher than bulk soil SOC at the mildly and moderately degraded stages (Fig. 2a). TN and TP were significantly enriched in rhizosphere soil from the undegraded to moderately degraded stages. However, this rhizosphere enrichment effect narrowed at the severely degraded stage (Fig. 2b, c).

In terms of enzymatic activities, rhizosphere soils exhibited significantly higher BG and Ppase activities than bulk soils regardless of the

Table 2
Soil physiochemical properties of rhizosphere and bulk soils in the three types of shelterbelt forests.

Tree species	Degradation stage	pH		SWC (%)		WSOC (mg/kg)		NH_4^+ (mg/kg)		NO_3^- (mg/kg)	
Soil zone		R	B	R	B	R	B	R	B	R	B
Populus popularis	1	7.42 ± 0.11a	8.15 ± 0.54a*	4.58 ± 0.99a	1.84 ± 0.25a*	0.058 ± 0.014a	0.049 ± 0.013a	2.26 ± 0.38a	1.67 ± 0.05a	5.84 ± 0.20a	5.16 ± 0.18a*
	2	8.45 ± 0.21b	9.26 ± 0.34b*	4.22 ± 1.48a	1.64 ± 0.47a*	0.054 ± 0.006a	0.033 ± 0.003b*	2.36 ± 0.35a	1.63 ± 0.24a	5.83 ± 0.25a	5.03 ± 0.12a*
	3	8.58 ± 0.18b	9.21 ± 0.19b*	2.54 ± 0.78b	1.75 ± 0.55a*	0.038 ± 0.004b	0.030 ± 0.001b*	2.10 ± 0.33a	1.60 ± 0.07a	5.29 ± 0.23b	5.22 ± 0.09a
	4	8.78 ± 0.24b	9.23 ± 0.10b*	1.86 ± 0.33b	1.90 ± 0.94a	0.041 ± 0.004b	0.036 ± 0.008ab	1.94 ± 0.53a	1.83 ± 0.45a	5.75 ± 0.27a	5.99 ± 0.88a
Populus thevestina	1	8.73 ± 0.17b	9.36 ± 0.16b*	5.14 ± 2.95a	2.05 ± 0.16a*	0.063 ± 0.016 a	0.041 ± 0.004a*	3.48 ± 2.40a	1.60 ± 0.07a	6.04 ± 0.29a	5.19 ± 0.28a*
	2	8.32 ± 0.03b	9.24 ± 0.09b*	2.84 ± 2.10ab	1.04 ± 0.14a*	0.061 ± 0.011 a	0.039 ± 0.005a*	3.38 ± 1.62a	1.42 ± 0.08a*	5.97 ± 0.63a	5.09 ± 0.14a*
	3	8.63 ± 0.15b	9.14 ± 0.06b*	6.27 ± 2.58a	4.48 ± 2.47b*	0.077 ± 0.019b	0.057 ± 0.013b*	6.62 ± 1.86b	2.55 ± 1.66b*	7.67 ± 0.24b	5.05 ± 0.32a *
	4	8.86 ± 0.10b	9.30 ± 0.04b*	1.61 ± 0.15b	1.07 ± 0.13a*	0.060 ± 0.005 a	0.049 ± 0.013ab	3.38 ± 0.45a	1.58 ± 0.10a*	6.34 ± 0.24a	4.99 ± 0.22a*
Populus alba	1	7.87 ± 0.02a	8.98 ± 0.04a*	3.70 ± 0.47a	1.16 ± 0.16a*	0.043 ± 0.006a	0.036 ± 0.002a	1.66 ± 0.33a	1.43 ± 0.09a	5.97 ± 0.16a	5.47 ± 0.45a
	2	7.87 ± 0.15a	9.20 ± 0.11b*	4.35 ± 0.92a	1.47 ± 0.94a*	0.048 ± 0.009a	0.039 ± 0.014a	1.73 ± 0.60a	1.44 ± 0.22a	6.07 ± 0.70a	5.40 ± 0.14a
	3	7.96 ± 0.30a	9.23 ± 0.15b*	2.98 ± 0.27a	1.07 ± 0.47a*	0.044 ± 0.010a	0.039 ± 0.008a	1.93 ± 0.17a	1.52 ± 0.14a	5.39 ± 0.58ab	5.44 ± 0.14a
	4	8.31 ± 0.33b	9.10 ± 0.25b*	2.70 ± 0.30a	1.37 ± 0.42a*	0.039 ± 0.006a	0.038 ± 0.007a	1.83 ± 0.17a	1.62 ± 0.07a	4.81 ± 0.83b	5.48 ± 0.08a

Note: all the data are expressed as mean ± standard deviation. Letter R refers to rhizosphere and letter B represents bulk soil. Lowercase letters show the significant differences among four degradation stages ($p < 0.05$). Asterisks represent significant differences between rhizosphere and bulk soil of the certain tree species and degradation stage ($p < 0.05$).

degradation stages (Fig. 2d, f). In contrast, rhizosphere NAG activity remained comparable to bulk soil levels at the undegraded and severely degraded stages, whereas it was significantly higher at the mildly and moderately degraded stages (Fig. 2e).

Regarding soil microbial biomass, MBC was higher in rhizosphere soil compared to bulk soil from undegraded to moderately degraded shelterbelt conditions, but this difference disappeared under the severely degraded stage (Fig. 2g). Similarly, rhizosphere soils had significantly higher MBN values than bulk soils during the first three degradation stages. However, this difference was no longer observed at the severely degraded stage (Fig. 2h). For MBP, no significant differences were found between rhizosphere and bulk soils throughout the entire degradation process, except at the mildly degraded stage where significantly higher values were observed in the rhizosphere compared to the bulk soil (Fig. 2i).

3.3. *Influencing factors associated with rhizosphere effects during shelterbelt degradation*

To explore factors associated with variations in REs across shelterbelt degradation gradients, we combined random forest and RDA analyses in a complementary manner. Random forest models showed that REs of soil C, N, and P pools were most strongly associated with nutrient concentrations and available N (mainly NO_3^-) in both rhizosphere and bulk soils (Fig. 3). For instance, the RE of TN was primarily predicted by the RE of MBN and bulk soil TN and TP, while the RE of TP showed high sensitivity to rhizosphere TP, bulk soil TP and RE of TN (Fig. 3). Enzyme-related REs exhibited weaker relationships, with the RE of BG linked mainly to MBP and bulk soil BG activity, whereas the RE of Ppase was closely associated with bulk soil Ppase activity. REs of microbial biomass showed strong internal coupling, with rhizosphere SWC emerging as a

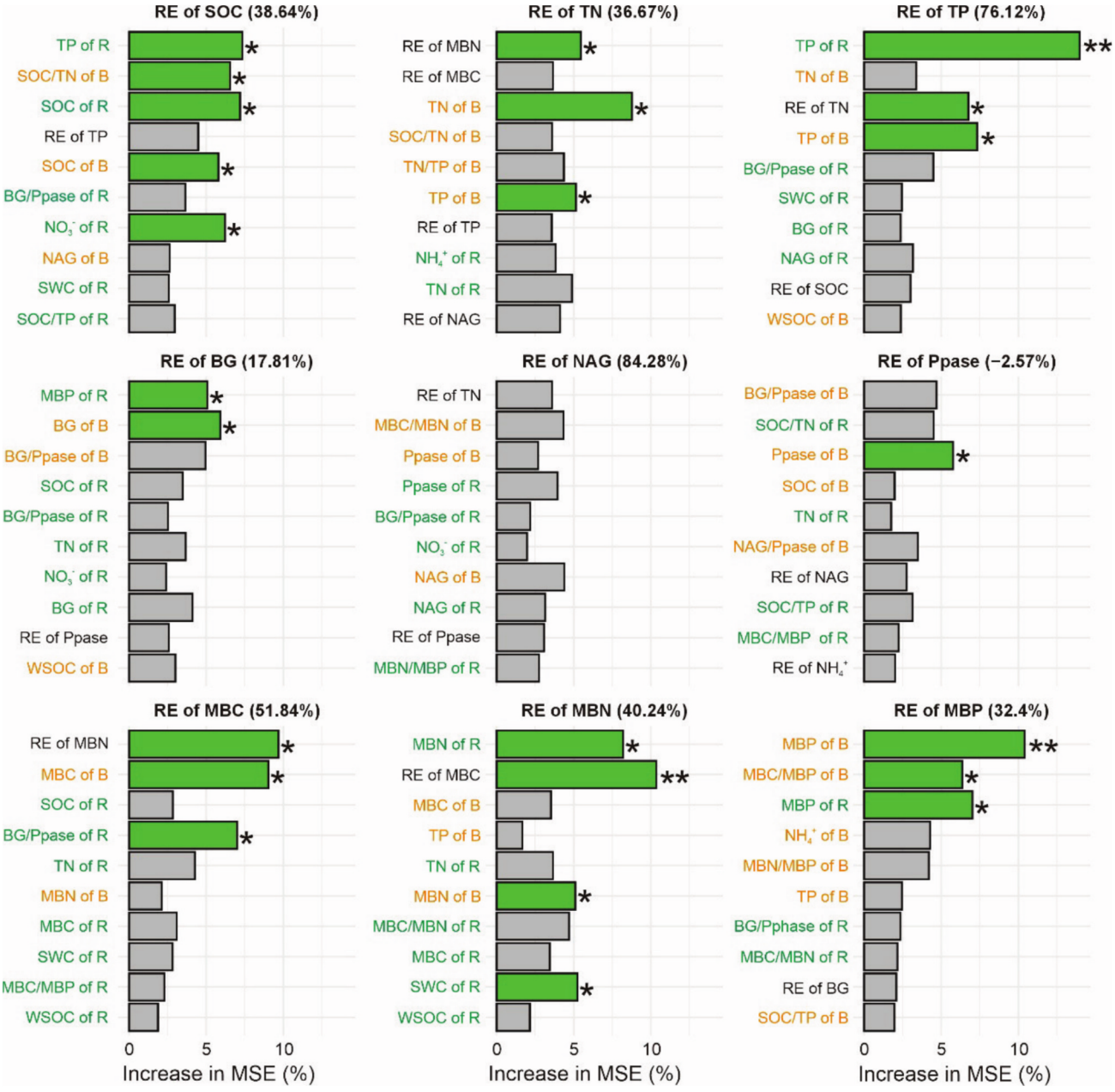

Fig. 3. The influential predictors of the rhizosphere effect of soil C, N, and P contents, soil enzymatic activities, and soil microbial biomass. Predictor variables include properties from rhizosphere soils (green), bulk soils (yellow), and RE-related traits (black). Double asterisk (**) indicates highly important variables (% IncMSE $>$ 10) and single asterisk (*) indicates moderately important variable (5 $<$ %IncMSE $\leq$ 10). Values in parentheses represent the proportion of variation explained for each corresponding response variable.

significant covariate, particularly for MBN (Fig. 3).

Based on these associations, top ten explanatory variables were selected for RDA analysis to summarize multivariate RE patterns while minimizing collinearity. In the overall ordination (Fig. 4a), the first two axes explained 81.39% of the total variance. Along RDA1, positive scores were aligned with stronger REs of microbial biomass (MBC, MBN, and MBP) and C- and N-acquiring enzymes (BG and NAG), which were positively associated with rhizosphere SWC, rhizosphere BG activity, bulk soil WSOC, and rhizosphere TN/TP ratio. This axis represents a coordinated enrichment of microbial biomass and enzyme-mediated nutrient processing in the rhizosphere. The second axis (RDA2) was primarily defined by the RE of Ppase, which loaded strongly in the negative direction, indicating a P-acquisition pattern distinct from overall microbial enrichment. Bulk soil TN was aligned with the RE of Ppase along RDA2, suggesting a potential coupling between P-acquisition strategies and soil N supply in response to soil stoichiometry. Clear separation among the three tree species was observed through species-level grouping (Fig. 4a). *Populus thevestina* clustered toward positive RDA1 values, indicating stronger composite rhizosphere enrichment of C and N pools. *Populus alba* occupied intermediate positions, whereas *Populus popularis* tended toward lower or negative RDA1 and lower RDA2 scores, suggesting weaker overall pool enrichment but a relatively greater emphasis on P-mining through phosphatase activity.

Species-specific ordinations further elucidated the divergent trajectories of the three poplar species along the degradation gradient (Fig. 4b–d). In *Populus popularis*, the rhizosphere response was characterized by a strong orientation toward the RE of Ppase during the early and moderate stages of degradation, whereas samples at the severely degraded stage shifted toward the opposite direction along RDA1 (Fig. 4b). In *Populus thevestina*, the REs of MBN, MBC, TN, and TP were positioned in the opposite direction of the REs of MBP and NAG. Furthermore, the RE of BG in this species was positively aligned with bulk soil WSOC (Fig. 4c). *Populus alba* followed a relatively stable trajectory, with its RE variables closely associated with variations in rhizosphere SWC, bulk soil WSOC, and rhizosphere BG activity throughout the degradation process (Fig. 4d). Across all three species, samples at the severe degradation stage consistently converged toward the origin or moved in the opposite direction of the RE vectors, signaling a comprehensive decline in the rhizosphere effect (Fig. 4).

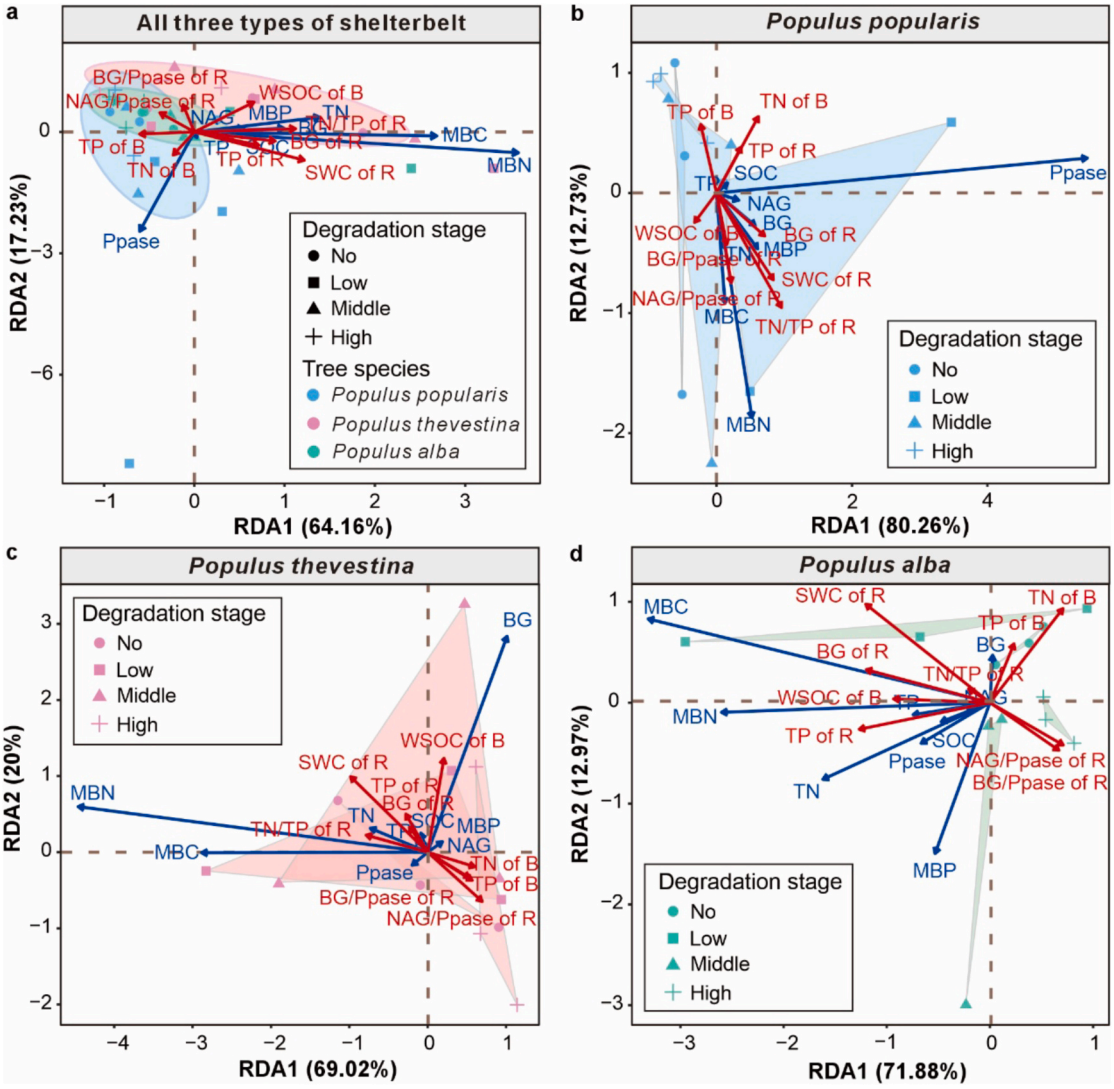

Fig. 4. Redundancy analysis (RDA) showing the relationships between rhizosphere effects and selected soil environmental variables across degradation stages. Panel a presents the overall ordination across all three Populus species, with ellipses indicating species-level grouping patterns, while Panels b, c, and d show species-specific ordinations for *Populus popularis*, *Populus thevestina*, and *Populus alba*, respectively. Degradation stages are indicated by different point shapes. Blue arrows represent rhizosphere effect variables, and red arrows represent selected soil environmental variables derived from rhizosphere (R) and bulk soil (B). The percentage of variance explained by each axis is indicated in parentheses.

4. Discussion

4.1. A hump-shaped rhizosphere response to shelterbelt degradation

Across soil nutrient pools (SOC, TN, TP), enzyme activities (BG, NAG, Ppase), and microbial biomass (MBC, MBN, MBP), the REs increased or remained stable from undegraded to mild-moderate degradation and then declined sharply at the severe degradation stage (Fig. 1). This nonlinear pattern was consistent across the three poplar shelterbelts, with species differing in magnitude and timing rather than direction. For example, *Populus thevestina* showed the largest early increases in REs of SOC, TN, and MBP, which peaked at moderately degraded stage and then fall back. In contrast, *Populus popularis* maintained comparatively high REs of BG and Ppase from the undegraded to mildly degraded stages (Fig. 1). In early stages, all REs were positive, reflecting a clear rhizosphere "hotspot" effect where rhizosphere values exceeded bulk soil (Fig. 2). This agrees with studies showing that rhizospheres commonly exhibit higher microbial abundance, hydrolytic activity, and MBC than adjacent bulk soil (Dotaniya and Meena, 2015; Zhao et al., 2022). This pattern also aligned with our observations of higher WSOC, available N ($NH_4^+$and NO_3^-), and SWC in rhizosphere soils (Table 2), microenvironment known to favor microbial growth, enzyme activity, and faster nutrient turnover (Neumann and Römheld, 2012; Angst et al., 2016; Mimmo et al., 2017). As degradation intensified, however, REs generally weakened toward zero and, for some variables (e.g., SOC and MBP in *Populus popularis*), turned to negative values (Fig. 1), revealing an overall hump-shaped trajectory.

The initial rise of REs might be explained as compensatory buffering of the root-soil system, representing a transient, stress-induced increase in rhizosphere functioning. During this period, plants tend to reallocate C and nutrients to roots and enhance root exudation to stimulate microbes and enzyme activities. Such plastic responses are documented for roots under nutrient addition (Hodge, 2004; Tong et al., 2025), altered precipitation (Zhou et al., 2019), and short-term drought (De Vries et al., 2016; Yin et al., 2023). For example, Williams and de Vries (2020) showed that under short-term/moderate drought, grasses increased root exudation and fungal abundance to keep normal growth rate, while under long-term/extreme drought the growth rate reduced with diminished root exudation and root-microbe interaction. Although many of these studies did not explicitly separate rhizosphere from bulk soil, the processes they described, such as exudation, foraging, and mycorrhizal mediation, operate mainly within the rhizosphere and therefore plausibly result as the temporary increase in the REs we observe during early degradation. These localized enhancements in rhizosphere, relative to bulk soil, indicate intensified belowground functioning during initial stress.

Beyond a tipping zone near the mid-degradation stage, this advantage of the rhizosphere soil eroded (Fig. 1, Fig. 2). Progressive canopy dieback and reduced physiological capacity likely curtailed nutrient and energy supply to roots and mycorrhizae, diminishing rhizodeposition and nutrient foraging (Lawlor and Tezara, 2009; Cao et al., 2024). Such concurrent nutrient limitation and physicochemical stress can substantially increase ecosystem vulnerability by amplifying the impacts of other biotic and abiotic stressors (Bal et al., 2015). The marked increase in soil pH and the significant decline in SWC and available N observed during the late degradation stages (Table 2) further support this, as the attenuation of root-driven acidification and nutrient priming leads to a more stressful microenvironment (Drenovsky et al., 2004; Stark et al., 2014). Critically, our results showed that the significant rhizosphere-bulk soil contrasts for SOC, TN, and microbial biomass (MBC, MBN, and MBP) completely disappeared at the severe degradation stage (Fig. 2). Nevertheless, the persistent significance of BG and Ppase activities (Fig. 2d, f) indicates that tree-driven regulation of the immediate rhizosphere remains functional before complete mortality, continuing to exert a positive, albeit weakened, influence on the rhizosphere microenvironment. This transition marks a shift from a buffered to a functionally collapsing rhizosphere as plant-soil feedbacks gradually weaken.

To sum up, these results reveal a nonlinear belowground trajectory. Early, root-driven buffering produces a transient peak in RE, followed by a sharp decline once degradation surpasses ecological thresholds (Fig. 5).

4.2. Drivers of the peak and fall of rhizosphere effect during shelterbelt degradation

REs are widely recognized as immediate outcomes of plant C allocation strategies, microbial activity, and the physicochemical environment at the root-soil interface (Kuzyakov and Razavi, 2019; Hartmann et al., 2020). In healthy shelterbelt, higher TN, TP, SWC, WSOC, and available N concentrations in rhizosphere soils coincided with positive REs for SOC, TN, TP, and enzyme activities (Fig. 1, Fig. 2). This pattern is consistent with previous studies showing that higher soil moisture stimulates microbial activity and enhances the solubility of SOC and inorganic P in dryland soils (Sherrod et al., 2018; De-Bashan et al., 2022), which maintains nutrient transport and root uptake, creating positive REs.

Under initial environmental stress, plants often prioritize maintaining metabolic stability and growth by reallocating readily available C to the root system (Arsova et al., 2020; Holz et al., 2024). For example, Savage et al. (2016) demonstrated that plants can adjust phloem physiology to modulate C allocation and increase carbohydrate supply to roots. This strategy potentially enhances root exudation and sustains rhizosphere microbial activity even as tree vigor begins to decline. Consistent with this, we observed elevated microbial biomass (Figs. 1, 2), higher MBC/MBN ratios, and strong coupling between soil microbial biomass and enzyme activities in early degradation stages (Figs. 3, 4). Our RDA results further support this buffering mechanism, as samples from early to moderate stages clustered along the vectors of rhizosphere SWC, WSOC, and nutrient-acquiring enzymes (Fig. 4). These processes amplify rhizosphere-bulk soil contrasts, creating the transient peak in REs observed across all three types of shelterbelts.

As degradation intensifies, rhizosphere conditions deteriorate, marked by rising pH and declining WSOC (Table 2). Reduced WSOC, a proxy for labile C availability, likely indicates C starvation for rhizosphere microbes in these C-poor sandy soils (Drenovsky et al., 2004; Choi et al., 2022), leading to the observed collapse in microbial biomass (MBC, MBN, MBP; Figs. 1, 2) and reduced N mineralization (reduced NH_4^+ and NO_3^-; Table 2). The RDA highlights the strong influence of bulk soil stoichiometry (TN, TP, and TN/TP of bulk soil) on REs, particularly for Ppase (Fig. 3, Fig. 4a). While plants initially invest in P-enzyme production to mitigate P limitation, as indicated by the alignment of Ppase with bulk soil TN (Fig. 4), the eventual depletion of C substrates undermines this response (Zhang et al., 2020, 2024). Consequently, the rhizosphere shifts from a buffered hotspot to a state limited by bulk-soil resource scarcity.

The three shelterbelt types exhibited similar trajectories but with species-specific adaptive strategies (Fig. 1, Fig. 4a). The stronger early REs in *Populus thevestina* are consistent with traits commonly associated with fast-growing poplar species, involving high belowground C allocation and aggressive nutrient foraging, as evidenced by its clustering toward the positive end of RDA1 (Fig. 4a, c). In contrast, *Populus popularis* maintained comparatively high REs for NAG and Ppase at early degradation stages (Fig. 4a, b), which, combined with the N limitation status of popular shelterbelt in northern China (Wang et al., 2024), suggesting a targeted investment toward nutrient-mining microbes rather than broad pool enrichment (Zhu et al., 2023). *Populus alba* displayed a delayed tipping point, with declines in REs for N- and P-related properties such as TN, NAG, TP, and MBP, occurring mainly at the moderately degraded stage (Fig. 1, Fig. 4d). The temporal lag of N- and P-related responses relative to C-related properties suggests that C limitation may emerge as the primary constraint earlier in the degradation

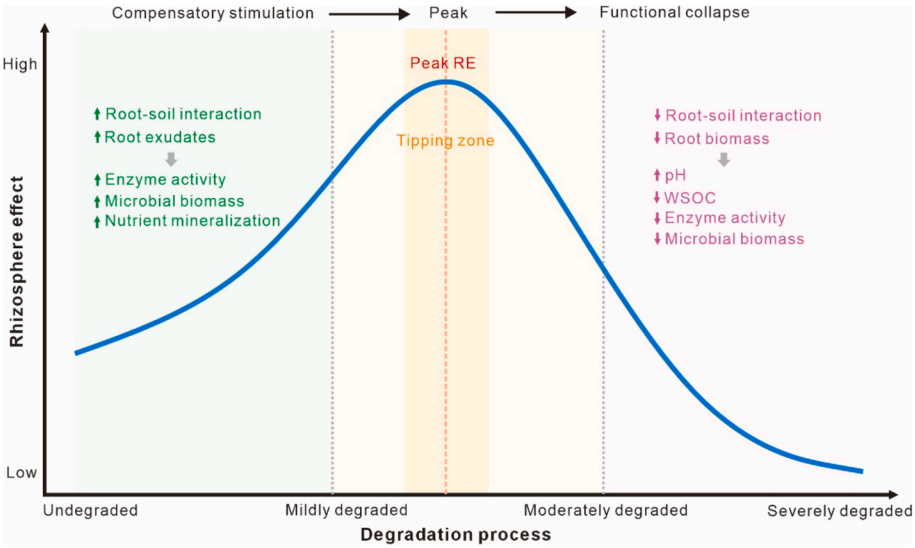

Fig. 5. Conceptual synthesis of rhizosphere responses to shelterbelt forest degradation. Early degradation triggers compensatory stimulation (↑increased root-soil interactions and exudation), temporarily increasing enzyme activity, microbial biomass, and nutrient mineralization, producing a peak rhizosphere effect (RE) near a tipping zone. With further degradation, feedbacks weaken and functional collapse occurs (↓root biomass and mycorrhizae, ↑pH, ↓WSOC, ↓enzyme activity and ↓microbial biomass). Shadings with different colors indicate phases along the degradation process.

sequence for *Populus alba*. As microbial mining of organic N and P is strictly energy-dependent (Finzi et al., 2015; Barba et al., 2016), the decline in N- and P-related REs only appears after a critical reduction in labile C availability and a deteriorating microenvironment (Table 2).

Combined, these results support a two-phase conceptual sequence of rhizosphere response to degradation (Fig. 5). First is the buffering phase, characterized by sufficient C substrate and favorable microclimatic conditions (high SWC, low pH), together with accessible P and N released from microbial activities, producing strong, positive REs (Fig. 5). Phase 2 is the decline phase, when rising pH and falling WSOC and SWC cross a physiological threshold. At this stage, inadequate photosynthesis caused C hunger, while concurrent bulk-soil nutrient scarcity and stoichiometric imbalance limit the replenishment of SOC and nutrients to rhizosphere (Bandopadhyay et al., 2024; Schultes et al., 2025). These factors collectively narrow the differences between rhizosphere and bulk soil.

4.3. Rhizosphere-bulk soil divergence and its implications for shelterbelt management

Across multiple soil variables, the contrast between rhizosphere and bulk soils increased from undegraded to mildly and moderately degraded stages, then narrowed under severe degradation (Fig. 1, Fig. 2, Table 2). In the early stages, higher WSOC, NH_4^+, NO_3^-, and SWC, along with slightly lower pH in the rhizosphere (Table 2), stimulated microbial biomass and hydrolytic enzyme activities, resulting in positive REs for C and nutrient pools. These localized enhancements suggest an active buffering phase where roots respond to stress by reallocating assimilates belowground to maintain the rhizosphere hotspot (Manzoni et al., 2012; Williams and de Vries, 2020). However, as degradation intensifies, canopy dieback reduces photosynthetic capacity (Crous et al., 2025), thereby limiting the supply of assimilates to the roots and diminishing rhizodeposition. Such reductions in belowground carbon inputs have been observed not only in poplar shelterbelts here but also in other forest types, such as subalpine coniferous forests (Weintraub et al., 2007). Concurrently, rising pH and declining WSOC and soil moisture constrain microbial activity. Collectively, these factors lead to a convergence of the rhizosphere toward bulk soil, represented by smaller or even negative REs, indicating the loss of the rhizosphere's advantage and microbial hotspots. This trajectory identifies RE as a leading indicator of belowground resilience. The gap between rhizosphere and bulk soil expands when buffering capacity is active and contracts as plant-soil feedbacks fail.

In light of these findings, we propose several management strategies to sustain rhizosphere function and prevent plant functional collapse. First, we suggest developing a composite RE index to track the rhizosphere-bulk soil contrast through time, and identify the tipping zone where RE plateaus before decline (Fig. 5). This would enable early detection of declining resilience. Second, management should prioritize practices that support rhizosphere activity, such as maintaining organic inputs to stabilize SOC and WSOC, implementing localized irrigation to the rhizosphere zone to maintain SWC, and favoring mycorrhiza-friendly practices (e.g., reduced disturbance). Furthermore, in N-limited shelterbelts, low-dose localized N inputs can support enzyme-mediated acquisition while minimizing environmental impacts. Species that exhibit strong rhizosphere enhancement under mild stress (e.g., high exudation or foraging capacity) may be more suitable for shelterbelt renewal.

To sum up, our study infers trajectories along a degradation gradient of commonly used poplar shelterbelts in dryland ecosystems. While many soil physicochemical and biological properties were examined to characterize these trajectories, certain key processes were not directly quantified. Specifically, the lack of direct measurements for root exudation means that the precise metabolic mechanisms driving the observed RE dynamics remain inferred. Future work should (i) pair manipulative experiments (water, WSOC, and P additions; controlled pH shifts) with breakpoint analysis to test the proposed tipping zone; (ii) measure exudates (e.g., ^{13}C labelling) and mycorrhiza to link plant resources allocation to RE dynamics; and (iii) develop composite RE indicators suited to different soil types and shelterbelt species to assess the generality of these findings across dryland ecosystems.

5. Conclusion

This study provides the first field-based evidence that the RE follows a non-linear, hump-shaped trajectory along shelterbelt forest degradation. We identified an early compensatory buffering phase, characterized by a peak in REs across C-N-P pools, soil enzymes, and microbial biomass near a critical tipping zone, followed by a functional collapse phase as REs declined sharply under severe degradation. This pattern

was consistent across three widely planted *Populus* species, which differed primarily in the amplitude and timing of their responses rather than the overall direction. The initial rise of REs was driven by a localized rhizosphere environment with lower pH and higher WSOC, inorganic N, and soil moisture, which stimulated microbial biomass and accelerated C-N-P cycling. Conversely, the subsequent fall of REs aligned with rising pH, declining WSOC, and increasing resource constraints from bulk soil nutrient stoichiometry. Collectively, these findings establish the rhizosphere as a leading indicator of belowground resilience. Practically, we recommend implementing a composite RE index to identify the tipping zone and time restoration interventions aimed at sustaining root functionality. By pinpointing the conditions under which rhizosphere advantages are gained and lost, this study provides a mechanistic framework and an actionable window for the conservation and restoration of shelterbelt ecosystems in dryland regions.

Declaration of Generative AI and AI-assisted technologies in the writing process

During the preparation of this work the authors used ChatGPT 5 to check grammar. After using this tool, the authors reviewed and edited the content as needed and take full responsibility for the content of the published article.

CRediT authorship contribution statement

Guan Wang: Writing – review & editing, Writing – original draft, Supervision, Resources, Funding acquisition, Formal analysis, Conceptualization. **Huijie Xiao:** Writing – review & editing, Resources, Project administration, Funding acquisition. **Linlin Shi:** Writing – review & editing, Software, Formal analysis, Data curation. **Tianshuo Liu:** Writing – review & editing, Validation, Investigation, Data curation. **Chenxi Yang:** Writing – review & editing, Investigation, Data curation. **Zhiming Xin:** Writing – review & editing, Visualization, Project administration. **Junran Li:** Writing – review & editing, Resources, Project administration.

Declaration of competing interest

The authors declare that they have no known competing financial interests or personal relationships that could have appeared to influence the work reported in this paper.

Acknowledgements

This work was supported by the Leader Project of Inner Mongolia Autonomous Region, “Technologies and Demonstration for the Construction of High-Standard Shelterbelt Systems in the Hetao Plain” [2024JBGS0002-1-02]. The authors sincerely thank the staff of Dengkou Desert Ecosystem National Observation Research Station for their assistance in field survey.

Appendix A. Supplementary material

Supplementary data to this article can be found online at https://doi.org/10.1016/j.geoderma.2026.117816.

Data availability

Original data can be found at https://data.mendeley.com/datasets/gcv2wxdgbr/1.

References

Angst, G., Kögel-Knabner, I., Kirfel, K., Hertel, D., Mueller, C.W., 2016. Spatial distribution and chemical composition of soil organic matter fractions in rhizosphere and non-rhizosphere soil under European beech (*Fagus sylvatica* L.). Geoderma 264, 179–187. https://doi.org/10.1016/j.geoderma.2015.10.016.

Anderegg, W.R., Berry, J.A., Smith, D.D., Sperry, J.S., Anderegg, L.D., Field, C.B., 2012. The roles of hydraulic and carbon stress in a widespread climate-induced forest die-off. Proc. Natl. Acad. Sci. 109 (1), 233–237. https://doi.org/10.1073/pnas.1107891109.

Arsova, B., Foster, K.J., Shelden, M.C., Bramley, H., Watt, M., 2020. Dynamics in plant roots and shoots minimize stress, save energy and maintain water and nutrient uptake. New Phytol. 225 (3), 1111–1119. https://doi.org/10.1111/nph.15955.

Ashraf, M.N., Hu, C., Wu, L., Duan, Y., Zhang, W., Aziz, T., Cai, A., Abrar, M., Xu, M., 2020. Soil and microbial biomass stoichiometry regulate soil organic carbon and nitrogen mineralization in rice-wheat rotation subjected to long-term fertilization. J. Soil. Sediment. 20 (8), 3103–3113. https://doi.org/10.1007/s11368-020-02642-y.

Bal, T.L., Storer, A.J., Jurgensen, M.F., Doskey, P.V., Amacher, M.C., 2015. Nutrient stress predisposes and contributes to sugar maple dieback across its northern range: a review. For. Int. J. For. Res. 88 (1), 64–83. https://doi.org/10.1093/forestry/cpu051.

Baldrian, P., 2017. Forest microbiome: diversity, complexity and dynamics. FEMS Microbiol. Rev. 41 (2), 109–130. https://doi.org/10.1093/femsre/fuw040.

Bandopadhyay, S., Li, X., Bowsher, A.W., Last, R.L., Shade, A., 2024. Disentangling plant- and environment-mediated drivers of active rhizosphere bacterial community dynamics during short-term drought. Nat. Commun. 15 (1), 6347. https://doi.org/10.1038/s41467-024-50463-1.

Barba, J., Lloret, F., Yuste, J.C., 2016. Effects of drought-induced forest die-off on litter decomposition. Plant Soil 402 (1), 91–101. https://doi.org/10.1007/s11104-015-2762-4.

Barillot, C.D., Sarde, C.O., Bert, V., Tarnaud, E., Cochet, N., 2013. A standardized method for the sampling of rhizosphere and rhizoplan soil bacteria associated to a herbaceous root system. Ann. Microbiol. 63 (2), 471–476. https://doi.org/10.1007/s13213-012-0491-y.

Bates, D., Mächler, M., Bolker, B., Walker, S., 2015. Fitting linear mixed-effects models using lme4. J. Stat. Softw. 67 (1), 1–48. https://doi.org/10.18637/jss.v067.i01.

Bouwmeester, H., Dong, L., Wippel, K., Hofland, T., Smilde, A., 2025. The chemical interaction between plants and the rhizosphere microbiome. Trends Plant Sci. https://doi.org/10.1016/j.tplants.2025.06.001.

Brandle, J.R., Takle, E., Zhou, X., 2021. Windbreak practices. North Am. Agrofor. 89–126. https://doi.org/10.1002/9780891183785.ch5.

Brunn, M., Hafner, B.D., Zwetsloot, M.J., Weikl, F., Pritsch, K., Hikino, K., Ruehr, N., Sayer, E., Bauerle, T.L., 2022. Carbon allocation to root exudates is maintained in mature temperate tree species under drought. New Phytol. 235 (3), 965–977. https://doi.org/10.1111/nph.18157.

Brunn, M., Mueller, C.W., Chari, N.R., Meier, I.C., Obersteiner, S., Phillips, R.P., Taylor, B., Tumber-Dávila, S.J., Ullah, S., Klein, T., 2025. Tree carbon allocation to root exudates: implications for carbon budgets, soil sequestration and drought response. Tree Physiol. 45 (4), tpaf026. https://doi.org/10.1093/treephys/tpaf026.

Cao, Q., Li, J., Wang, G., Wang, D., Xin, Z., Xiao, H., Zhang, K., 2021. On the spatial variability and influencing factors of soil organic carbon and total nitrogen stocks in a desert oasis ecotone of northwestern China. Catena 206, 105533. https://doi.org/10.1016/j.catena.2021.105533.

Cao, Q., Zhou, Y., Bai, Y., Han, Z., 2024. Available nitrogen and enzyme activity in rhizosphere soil dominate the changes in fine-root nutrient foraging strategies during plantation development. Geoderma 446, 116901. https://doi.org/10.1016/j.geoderma.2024.116901.

Chen, Z., Xiao, Y., Dong, X., Deng, Z., Zhou, X., Yan, G., Zhang, J., Han, S., 2025. Nitrogen addition promotes soil organic phosphorus accumulation through increasing microbial biomass phosphorus in a temperate forest. Plant Soil 511 (1), 1433–1448. https://doi.org/10.1007/s11104-024-07064-0.

Cheng, Y., Zhan, H., Yang, W., Jiang, Q., Wang, Y., Guo, F., 2021. An ecohydrological perspective of reconstructed vegetation in the semi-arid region in drought seasons. Agric. Water Manag. 243, 106488. https://doi.org/10.1016/j.agwat.2020.106488.

Chirwa, P.W., Mahamane, L., 2017. Overview of restoration and management practices in the degraded landscapes of the Sahelian and dryland forests and woodlands of East and southern Africa. South. For. J. For. Sci. 79 (2), 87–94. https://doi.org/10.2989/20702620.2016.1255419.

Choi, R.T., Reed, S.C., Tucker, C.L., 2022. Multiple resource limitation of dryland soil microbial carbon cycling on the Colorado Plateau. Ecology 103 (6), e3671.

Clausing, S., Pena, R., Song, B., Müller, K., Mayer-Gruner, P., Marhan, S., Grafe, M., Schulz, S., Krüger, J., Lang, F., Schloter, M., 2021. Carbohydrate depletion in roots impedes phosphorus nutrition in young forest trees. New Phytol. 229 (5), 2611–2624. https://doi.org/10.1111/nph.17058.

Cross, M.S., Harte, J., 2007. Compensatory responses to loss of warming-sensitive plant species. Ecology 88 (3), 740–748. https://doi.org/10.1890/06-1029.

Crous, K.Y., Middleby, K.B., Cheesman, A.W., Bouet, A.Y., Schiffer, M., Liddell, M.J., Barton, C.V., Cernusak, L.A., 2025. Leaf warming in the canopy of mature tropical trees reduced photosynthesis due to downregulation of photosynthetic capacity and reduced stomatal conductance. New Phytol. 245 (4), 1421–1436. https://doi.org/10.1111/nph.20320.

De Vries, F.T., Brown, C., Stevens, C.J., 2016. Grassland species root response to drought: consequences for soil carbon and nitrogen availability. Plant Soil 409 (1), 297–312. https://doi.org/10.1007/s11104-016-2964-4.

De-Bashan, L.E., Magallon-Servin, P., Lopez, B.R., Nannipieri, P., 2022. Biological activities affect the dynamic of P in dryland soils. Biol. Fertil. Soils 58 (2), 105–119. https://doi.org/10.1007/s00374-021-01609-6.

Dotaniya, M.L., Meena, V.D., 2015. Rhizosphere effect on nutrient availability in soil and its uptake by plants: a review. Proc. Natl. Acad. Sci. India Sect. B Biol. Sci. 85 (1), 1–12. https://doi.org/10.1007/s40011-013-0297-0.

Drenovsky, R.E., Vo, D., Graham, K.J., Scow, K.M., 2004. Soil water content and organic carbon availability are major determinants of soil microbial community composition. Microb. Ecol. 48 (3), 424–430. https://doi.org/10.1007/s00248-003-1063-2.

Finzi, A.C., Abramoff, R.Z., Spiller, K.S., Brzostek, E.R., Darby, B.A., Kramer, M.A., Phillips, R.P., 2015. Rhizosphere processes are quantitatively important components of terrestrial carbon and nutrient cycles. Glob. Chang. Biol. 21 (5), 2082–2094. https://doi.org/10.1111/gcb.12816.

Freschet, G.T., Roumet, C., Comas, L.H., Weemstra, M., Bengough, A.G., Rewald, B., Bardgett, R.D., De Deyn, G.B., Johnson, D., Klimešová, J., Lukac, M., McCormack, M. L., Meier, I.C., Pagès, L., Poorter, H., Prieto, I., Wurzburger, N., Zadworny, M., Bagniewska-Zadworna, A., Blancaflor, E.B., Brunner, I., Gessler, A., Hobbie, S.E., Iversen, C.M., Mommer, L., Picon-Cochard, C., Postma, J.A., Rose, L., Ryser, P., Scherer-Lorenzen, M., Soudzilovskaia, N.A., Sun, T., Valverde-Barrantes, O.J., Weigelt, A., York, L.M., Stokes, A., 2021. Root traits as drivers of plant and ecosystem functioning: current understanding, pitfalls and future research needs. New Phytol. 232 (3), 1123–1158. https://doi.org/10.1111/nph.17072.

Friggens, N.L., Hugelius, G., Kokelj, S.V., Murton, J.B., Phoenix, G.K., Hartley, I.P., 2025. Positive rhizosphere priming accelerates carbon release from permafrost soils. Nat. Commun. 16 (1), 3576. https://doi.org/10.1038/s41467-025-58845-9.

George, T.S., Bulgarelli, D., Carminati, A., Chen, Y., Jones, D., Kuzyakov, Y., Schnepf, A., Wissuwa, M., Roose, T., 2024. Bottom-up perspective–the role of roots and rhizosphere in climate change adaptation and mitigation in agroecosystems. Plant Soil 500 (1), 297–323. https://doi.org/10.1007/s11104-024-06626-6.

German, D.P., Weintraub, M.N., Grandy, A.S., Lauber, C.L., Rinkes, Z.L., Allison, S.D., 2011. Optimization of hydrolytic and oxidative enzyme methods for ecosystem studies. Soil Biol. Biochem. 43 (7), 1387–1397. https://doi.org/10.1016/j.soilbio.2011.03.017.

Hartmann, H., Bahn, M., Carbone, M., Richardson, A.D., 2020. Plant carbon allocation in a changing world–challenges and progress. New Phytol. 227 (4), 981–988. https://www.jstor.org/stable/26928211.

Hendel, B., Marxsen, J., 2020. Fluorometric determination of the activity of β-glucosidase and other extracellular hydrolytic enzymes. In: Methods to Study Litter Decomposition: a Practical Guide. Springer International Publishing, Cham, pp. 411–418.

Herre, M., Heitkötter, J., Heinze, S., Rethemeyer, J., Preusser, S., Kandeler, E., Marschner, B., 2022. Differences in organic matter properties and microbial activity between bulk and rhizosphere soil from the top-and subsoils of three forest stands. Geoderma 409, 115589. https://doi.org/10.1016/j.geoderma.2021.115589.

Hill, P.W., Jones, D.L., 2019. Plant–microbe competition: does injection of isotopes of C and N into the rhizosphere effectively characterise plant use of soil N? New Phytol. 221 (2), 796–806. https://www.jstor.org/stable/26557255.

Hodge, A., 2004. The plastic plant: root responses to heterogeneous supplies of nutrients. New Phytol. 162 (1), 9–24. https://doi.org/10.1111/j.1469-8137.2004.01015.x.

Holz, M., Zarebanadkouki, M., Benard, P., Hoffmann, M., Dubbert, M., 2024. Root and rhizosphere traits for enhanced water and nutrients uptake efficiency in dynamic environments. Front. Plant Sci. 15, 1383373. https://doi.org/10.3389/fpls.2024.1383373.

IUSS Working Group WRB, 2022. World Reference Base for Soil Resources. International soil classification system for naming soils and creating legends for soil maps, 4th ed. International Union of Soil Sciences (IUSS), Vienna, Austria.

Jones, D.L., Nguyen, C., Finlay, R.D., 2009. Carbon flow in the rhizosphere: carbon trading at the soil-root interface. Plant Soil 321, 5–33. https://doi.org/10.1007/s11104-009-9925-0.

Kuznetsova, A., Brockhoff, P.B., Christensen, R.H.B., 2017. lmerTest package: tests in linear mixed effects models. J. Stat. Softw. 82 (13), 1–26. https://doi.org/10.18637/jss.v082.i13.

Kuzyakov, Y., Razavi, B.S., 2019. Rhizosphere size and shape: temporal dynamics and spatial stationarity. Soil Biol. Biochem. 135, 343–360. https://doi.org/10.1016/j.soilbio.2019.05.011.

Lambers, H., Mougel, C., Jaillard, B., Hinsinger, P., 2009. Plant-microbe-soil interactions in the rhizosphere: an evolutionary perspective. Plant Soil 321, 83–115. https://doi.org/10.1007/s11104-009-0042-x.

Lawlor, D.W., Tezara, W., 2009. Causes of decreased photosynthetic rate and metabolic capacity in water-deficient leaf cells: a critical evaluation of mechanisms and integration of processes. Ann. Bot. 103 (4), 561–579. https://doi.org/10.1093/aob/mcn244.

Lenth, R., Piaskowski, J., 2026. emmeans: Estimated Marginal Means, aka Least-Squares Means. R package version 2.0. https://CRAN.R-project.org/package=emmeans.

Liang, X., Xin, Z., Liu, S., Shen, H., Zhang, Z., 2024. Determination of plantation degradation promotes shallow soil water recovery in semi-arid area based on high-density plots investigation. Geoderma 443, 116839. https://doi.org/10.1016/j.geoderma.2024.116839.

Liang, X., Xin, Z., Shen, H., Yan, T., 2022. Deep soil water deficit causes Populus simonii Carr degradation in the three north shelterbelt region of China. J. Hydrol. 612, 128201. https://doi.org/10.1016/j.jhydrol.2022.128201.

Liaw, A., Wiener, M., 2002. Classification and regression by randomForest. R News 2 (3), 18–22. https://CRAN.R-project.org/doc/Rnews/.

Ling, N., Wang, T., Kuzyakov, Y., 2022. Rhizosphere bacteriome structure and functions. Nat. Commun. 13 (1), 836. https://doi.org/10.1038/s41467-022-28448-9.

Liu, Z., Jia, G., Yu, X., 2020. Variation of water uptake in degradation agroforestry shelterbelts on the North China Plain. Agric. Ecosyst. Environ. 287, 106697. https://doi.org/10.1016/j.agee.2019.106697.

Lv, C., Wang, C., Cai, A., Zhou, Z., 2023. Global magnitude of rhizosphere effects on soil microbial communities and carbon cycling in natural terrestrial ecosystems. Sci. Total Environ. 856, 158961. https://doi.org/10.1016/j.scitotenv.2022.158961.

Manzoni, S., Schimel, J.P., Porporato, A., 2012. Responses of soil microbial communities to water stress: results from a meta-analysis. Ecology 93 (4), 930–938. https://doi.org/10.1890/11-0026.1.

Marais, Z.E., Baker, T.P., Hunt, M.A., Mendham, D., 2022. Shelterbelt species composition and age determine structure: consequences for ecosystem services. Agric. Ecosyst. Environ. 329, 107884. https://doi.org/10.1016/j.agee.2022.107884.

Meier, I.C., Brunner, I., Godbold, D.L., Helmisaari, H.S., Ostonen, I., Soudzilovskaia, N. A., Prescott, C.E., 2019. Roots and rhizospheres in forest ecosystems: recent advances and future challenges. For. Ecol. Manage. 431, 1–5. https://doi.org/10.1016/j.foreco.2018.08.005.

Meier, I.C., Pritchard, S.G., Brzostek, E.R., McCormack, M.L., Phillips, R.P., 2015. The rhizosphere and hyphosphere differ in their impacts on carbon and nitrogen cycling in forests exposed to elevated CO_2. New Phytol. 205 (3), 1164–1174. https://doi.org/10.1111/nph.13122.

Millard, P., Sommerkorn, M., Grelet, G.A., 2007. Environmental change and carbon limitation in trees: a biochemical, ecophysiological and ecosystem appraisal. New Phytol. 175 (1), 11–28. https://doi.org/10.1111/j.1469-8137.2007.02079.x.

Mimmo, T., Pii, Y., Valentinuzzi, F., Astolfi, S., Lehto, N., Robinson, B., Brunetto, G., Terzano, R., Cesco, S., 2017. Nutrient availability in the rhizosphere: a review. In: VIII International Symposium on Mineral Nutrition of Fruit Crops, pp. 13–28. https://doi.org/10.17660/ActaHortic.2018.1217.2.

Mori, A.S., Furukawa, T., Sasaki, T., 2013. Response diversity determines the resilience of ecosystems to environmental change. Biol. Rev. 88 (2), 349–364. https://doi.org/10.1111/brv.12004.

Neumann, G., Römheld, V., 2012. Rhizosphere chemistry in relation to plant nutrition. In: Marschner's Mineral Nutrition of Higher Plants. Academic Press, pp. 347–368.

Oksanen, J., Blanchet, F.G., Friendly, M., Kindt, R., Legendre, P., McGlinn, D., Minchin, P.R., O'Hara, R.B., Simpson, G.L., Solymos, P., Stevens, M.H.H., Szoecs, E., Wagner, H., 2024. vegan: Community Ecology Package. R package version 2.6-6. https://CRAN.R-project.org/package=vegan.

Pett-Ridge, J., Firestone, M.K., 2017. Using stable isotopes to explore root-microbe-mineral interactions in soil. Rhizosphere 3, 244–253. https://doi.org/10.1016/j.rhisph.2017.04.016.

Pii, Y., Mimmo, T., Tomasi, N., Terzano, R., Cesco, S., Crecchio, C., 2015. Microbial interactions in the rhizosphere: beneficial influences of plant growth-promoting rhizobacteria on nutrient acquisition process. A review. Biol. Fertil. Soils 51 (4), 403–415. https://doi.org/10.1007/s00374-015-0996-1.

Preece, C., Peñuelas, J., 2016. Rhizodeposition under drought and consequences for soil communities and ecosystem resilience. Plant Soil 409 (1), 1–17. https://doi.org/10.1007/s11104-016-3090-z.

Prescott, C.E., 2022. Sinks for plant surplus carbon explain several ecological phenomena. Plant Soil 476 (1), 689–698. https://doi.org/10.1007/s11104-022-05390-9.

R Core Team, 2024. R: A language and environment for statistical computing (Version 4.3.3). R Foundation for Statistical Computing, Vienna, Austria. https://www.R-project.org/.

Robert, C.A., Ferrieri, R.A., Schirmer, S., Babst, B.A., Schueller, M.J., Machado, R.A., Arce, C.C.M., Hibbard, B.E., Gershenzon, J., Turlings, T.C.J., Erb, M., 2014. Induced carbon reallocation and compensatory growth as root herbivore tolerance mechanisms. Plant Cell Environ. 37 (11), 2613–2622. https://doi.org/10.1111/pce.12359.

Sardans, J., Peñuelas, J., 2013. Plant-soil interactions in Mediterranean forest and shrublands: impacts of climatic change. Plant Soil 365 (1), 1–33. https://doi.org/10.1007/s11104-013-1591-6.

Savage, J.A., Clearwater, M.J., Haines, D.F., Klein, T., Mencuccini, M., Sevanto, S., Turgeon, R., Zhang, C., 2016. Allocation, stress tolerance and carbon transport in plants: how does phloem physiology affect plant ecology? Plant Cell Environ. 39 (4), 709–725. https://doi.org/10.1111/pce.12602.

Schultes, S.R., Rüger, L., Niedeggen, D., Freudenthal, J., Frindte, K., Becker, M.F., Metzner, R., Pflugfelder, D., Chlubek, A., Hinz, C., van Dusschoten, D., Bauke, S.L., Bonkowski, M., Watt, M., Koller, R., Knief, C., 2025. Photosynthate distribution determines spatial patterns in the rhizosphere microbiota of the maize root system. Nat. Commun. 16 (1), 7286. https://doi.org/10.1038/s41467-025-62550-y.

Scott, E., 2012. A3: accurate, adaptable, and accessible error metrics for predictive models. R package version 1.0.0. https://CRAN.R-project.org/package=A3.

Shen, X., Yang, F., Xiao, C., Zhou, Y., 2020. Increased contribution of root exudates to soil carbon input during grassland degradation. Soil Biol. Biochem. 146, 107817. https://doi.org/10.1016/j.soilbio.2020.107817.

Sherrod, L.A., McMaster, G.S., Delgado, J.A., Schipanski, M.E., Fonte, S.J., Montenieri, R. L., Larson, K., 2018. Soil carbon pools in dryland agroecosystems as affected by several years of drought. J. Environ. Qual. 47 (4), 766–773. https://doi.org/10.2134/jeq2017.09.0371.

Stark, S., Männistö, M.K., Eskelinen, A., 2014. Nutrient availability and pH jointly constrain microbial extracellular enzyme activities in nutrient-poor tundra soils. Plant Soil 383 (1), 373–385. https://doi.org/10.1007/s11104-014-2181-y.

Stevenson, B.A., Sarmah, A.K., Smernik, R., Hunter, D.W., Fraser, S., 2016. Soil carbon characterization and nutrient ratios across land uses on two contrasting soils: their relationships to microbial biomass and function. Soil Biol. Biochem. 97, 50–62. https://doi.org/10.1016/j.soilbio.2016.02.009.

Tong, R., Kuzyakov, Y., Yu, H., Cao, Y., Wu, T., 2025. Rhizosphere response and resistance to fertilization. Commun. Earth Environ. 6 (1), 602. https://doi.org/10.1038/s43247-025-02567-9.

Wang, G., Xiao, H., Xin, Z., Luo, F., Jin, Y., Liu, M., Li, J., 2024. Changes in plant-soil-microbe CNP contents and stoichiometry during poplar shelterbelt degradation. Catena 243, 108227. https://doi.org/10.1016/j.catena.2024.108227.

Weintraub, M.N., Scott-Denton, L.E., Schmidt, S.K., Monson, R.K., 2007. The effects of tree rhizodeposition on soil exoenzyme activity, dissolved organic carbon, and nutrient availability in a subalpine forest ecosystem. Oecologia 154 (2), 327–338. https://doi.org/10.1007/s00442-007-0804-1.

Wen, Y., Liu, B., Lin, L., Hu, M., Wen, X., Li, T.Y., Rong, J., Yao, S., 2024. Shelterbelt effects on soil redistribution on an arable slope by wind and water. Catena 241, 108044. https://doi.org/10.1016/j.catena.2024.108044.

Wickham, H., 2016. ggplot2: Elegant Graphics for Data Analysis. Springer-Verlag, New York, USA.

Wiley, E., 2020. Do carbon reserves increase tree survival during stress and following disturbance? Curr. For. Rep. 6 (1), 14–25. https://doi.org/10.1007/s40725-019-00106-2.

Williams, A., de Vries, F.T., 2020. Plant root exudation under drought: implications for ecosystem functioning. New Phytol. 225 (5), 1899–1905. https://doi.org/10.1111/nph.16223.

Wu, F., Yang, W., Sun, B., Yang, T., Chen, X., Xu, Z., Song, H., 2022. Soil C, N and P stocks and stoichiometry under different vegetation on the surface of the Leshan Giant Buddha. Soil Ecol. Lett. 4 (1), 69–77. https://doi.org/10.1007/s42832-020-0061-3.

Xie, H., Chang, M., Bao, B., Li, X., Wang, G.G., 2024. Linking canopy gap features and microhabitat heterogeneity with seedling regeneration in a mixed coastal shelterbelt forest of eastern China. For. Ecol. Manage. 571, 122259. https://doi.org/10.1016/j.foreco.2024.122259.

Yan, Y., Li, P., Wang, Z., Tan, Y., Zheng, T., Liu, J., Yang, X., Liu, J., 2025. A decision framework for rural domestic sewage treatment models and process: evidence from Inner Mongolia Autonomous Region, China. J. Environ. Sci. https://doi.org/10.1016/j.jes.2025.05.016.

Yin, S., Wang, C., Lv, C., Zhou, Z., 2023. Short-term responses of root traits and carbon exudation to drought in a Larix gmelinii plantation. Plant Soil 484 (1), 393–405. https://doi.org/10.1007/s11104-022-05800-y.

Yu, Q., Yue, D., Wang, Y., Kai, S., Fang, M., Ma, H., Zhang, Q., Huang, Y., 2018. Optimization of ecological node layout and stability analysis of ecological network in desert oasis: a typical case study of ecological fragile zone located at Deng Kou County (Inner Mongolia). Ecol. Ind. 84, 304–318. https://doi.org/10.1016/j.ecolind.2017.09.002.

Zhang, C., Zhang, X., Kuzyakov, Y., Wang, H., Fu, X., Yang, Y., Chen, F., Dungait, J., Green, S.M., Fang, X., 2020. Responses of C-, N-and P-acquiring hydrolases to P and N fertilizers in a subtropical Chinese fir plantation depend on soil depth. Appl. Soil Ecol. 150, 103465. https://doi.org/10.1016/j.apsoil.2019.103465.

Zhang, H., Liu, X., Long, J., Yang, T., Huo, H., Jia, C., Yi, L., Herath, S., Peng, X., 2024. Phosphorus addition stimulates overall carbon acquisition enzymes but suppresses overall phosphorus acquisition enzymes: a global meta-analysis. Agric. Ecosyst. Environ. 375, 109219. https://doi.org/10.1016/j.agee.2024.109219.

Zhang, P., Ding, J., Kong, D., Yin, H., 2026. Rhizospheric traits and plant functioning belowground. Plant Commun. 7 (1). https://doi.org/10.1016/j.xplc.2025.101579.

Zhang, Y., Wang, R., Sardans, J., Wang, B., Gu, B., Li, Y., Liu, H., Peñuelas, J., Jiang, Y., 2023. Resprouting ability differs among plant functional groups along a soil acidification gradient in a meadow: a rhizosphere perspective. J. Ecol. 111 (3), 631–644. https://doi.org/10.1111/1365-2745.14051.

Zhao, X., Tian, P., Sun, Z., Liu, S., Wang, Q., Zeng, Z., 2022. Rhizosphere effects on soil organic carbon processes in terrestrial ecosystems: a meta-analysis. Geoderma 412, 115739. https://doi.org/10.1016/j.geoderma.2022.115739.

Zhou, M., Wang, J., Bai, W., Zhang, Y., Zhang, W.H., 2019. The response of root traits to precipitation change of herbaceous species in temperate steppes. Funct. Ecol. 33 (10), 2030–2041. https://doi.org/10.1111/1365-2435.13420.

Zhu, J., Song, L., 2021. A review of ecological mechanisms for management practices of protective forests. J. For. Res. 32 (2), 435–448. https://doi.org/10.1007/s11676-020-01233-4.

Zhu, X., Lambers, H., Guo, W., Chen, D., Liu, Z., Zhang, Z., Yin, H., 2023. Extraradical hyphae exhibit more plastic nutrient-acquisition strategies than roots under nitrogen enrichment in ectomycorrhiza-dominated forests. Glob. Chang. Biol. 29 (16), 4605–4619. https://doi.org/10.1111/gcb.16768.